RSC Advances

PAPER

View Article Online
View Journal | View Issue

Cite this: *RSC Adv.*, 2017, **7**, 4848

Low-dielectric polyimide nanofoams derived from 4,4′-(hexafluoroisopropylidene)diphthalic anhydride and 2,2′-bis(trifluoromethyl)benzidine†

Pengxia Lv,[ab] Zhixin Dong,*[a] Xuemin Dai,[a] Yong Zhao[ab] and Xuepeng Qiu*[a]

Received 21st October 2016
Accepted 28th December 2016

DOI: 10.1039/c6ra25604j

www.rsc.org/advances

Low-dielectric polyimide (PI) nanofoams were prepared by introducing nanopores into the PI matrix containing fluorine groups. The nanopores were formed by thermolysis of the thermally labile content, namely, polyethylene glycol (PEG) oligomers, in air. The prepared PI nanofoams were characterized by Fourier transform infrared (FT-IR) spectroscopy, scanning electron microscopy (SEM), thermogravimetric analysis (TGA), dynamic mechanical analysis (DMA), and broadband dielectric spectroscopy. Results indicated that the PI nanofoams showed nanosized closed pores, excellent thermal stability, and a low dielectric constant of 2.12. The dielectric constant of the as-prepared nanofoams was stable within −150 °C to 150 °C. The thermal decomposition process of PEG in the PI matrix was designed and optimized to control the decomposition rate of PEG and the diffusion rate of the decomposition products of PEG. The dielectric constant of the nanofoams significantly decreased from 2.45 to 2.12 as the heating rate decreased from 5 °C min^{-1} to 1 °C min^{-1}. The as-prepared PI nanofoams exhibited excellent properties and thus could be used in the microelectronics industry as a dielectric layer, multi-chip modules, or integrated circuit chips.

1. Introduction

With the development of information technology and the microelectronics industry, the feature size of microelectronics devices has decreased while the density of wires on chips has increased, leading to circuit loss, signal distortion and delay.[1,2] Maex[3] reported that interconnect technology is a crucial factor affecting signal delay. These limitations could be resolved by decreasing the dielectric constant of insulation materials.

As pointed out by the international semiconductor industry association in the International Technology Roadmap for Semiconductors in 2009,[4] the dielectric constant of insulation materials applied in microelectronics devices should be less than 2.0. However, conventional insulation materials, such as SiO_2 and Si_3N_4, exhibit high dielectric constants (3.9 to 4.2). Therefore, ultra-low dielectric materials must be developed for the microelectronics field. Polyimide (PI) materials are high-performance polymer preferred in the microelectronics field because of their excellent mechanical property, thermal stability, chemical stability, adhesion, low water absorption, and dielectric constant.[5–7] However, the dielectric constant of traditional PI materials is between 3.0 and 3.4, which is too high to be used as an ultra-low dielectric constant insulator. Therefore, we should reduce the dielectric constant of PI materials. Generally, the dielectric constant of PI materials can be reduced through two methods: introduction of structural units with low molar polarizability or large molar volume to the macromolecular chain and taking of low-dielectric constant media, such as air, into the PI matrix.[3,8,9]

Since the 1990s, scientists at the research center of IBM have devoted themselves to obtain low-dielectric PI nanofoam materials.[10–15] PI nanofoams with low dielectric constant are prepared by incorporating nanopores into the PI matrix after thermolysis of the thermal labile part, which is grafted on the molecular chain or formed block copolymers with PI. Frequently used thermal unstable materials include polystyrene,[16] polypropylene oxide (PPO),[17–19] polymethylmethacrylate,[17,20] polycaprolactone,[21] and poly(α-methyl styrene) (PMS),[22] which are terminated by amino. All these thermally labile materials are decomposed into volatile small molecules, followed by escape after heating. Han *et al.*[23] and Mehdipour-Ataei *et al.*[24] prepared PI nanofoams with dielectric constant of 2.34 by thermal decomposition of the grafted poly(propylene glycol) (PPG) terminated with bromine. In contrast to grafting of thermally labile materials *via* amino-termination proposed by IBM, incorporating bromine-terminated PPG did not disturb the macromolecular structure of PI. In Kang's report,[25,26] reversible addition–fragmentation chain-transfer polymerization was adopted to graft the thermal labile content on the PI macromolecular chains, followed by

[a]*Polymer Composites Engineering Laboratory, Changchun Institute of Applied Chemistry, Chinese Academy of Sciences, Changchun 130022, P. R. China. E-mail: zxdong@ciac.ac.cn; xp_q@ciac.ac.cn; Fax: +86 431 85262095; Tel: +86 431 85262557*

[b]*University of Chinese Academy of Sciences, Beijing 100049, P. R. China*

† Electronic supplementary information (ESI) available. See DOI: 10.1039/c6ra25604j

thermal decomposition to obtain PI nanofoams. In this method, the molecular weight and distribution of grafted thermal labile polymers could be satisfactorily controlled to produce PI nanofoams with narrow nanopore distribution and low dielectric constant. Zhang *et al.*[27,28] reported a simple method, namely, direct addition of poly(ethylene) oxide to the PI matrix followed by thermolysis to prepare PI nanofoams with good thermal stability and a low dielectric constant of 2.4.

Although PI nanofoams with low dielectric constant can be prepared through various methods, the interactions between the PI matrix and decomposition products of thermal labile content have not been investigated yet; these interactions must be elucidated to avoid the plasticization of the PI matrix caused by decomposition products and the collapse of the nanopores. In the current work, a new simple system was designed and prepared to study the properties of nanofoams. Specifically, PI containing fluorine groups was used as matrix, and polyethylene glycol (PEG) oligomers with average molecular weights of 600 g mol^{-1} were adopted as thermal labile content to obtain PI nanofoams with low dielectric constant after thermal decomposition. The films foaming processes were designed to control the decomposition rate of the thermally unstable content and the diffusion rate of the decomposition products to investigate the above interactions extensively.

2. Experimental

2.1 Materials

4,4′-(Hexafluoroisopropylidene)diphthalic anhydride (6FDA) and 2,2′-bis(trifluoromethyl)benzidine (TFDB) were purchased from Aldrich and purified *via* heating and sublimation, respectively. PEG-600 (600 g mol^{-1} average molecular weight) and acetic anhydride were obtained from Sinopharm Chemical Reagent Co., Ltd. *N*,*N*′-Dimethylacetamide (DMAc) and triethylamine were supplied by Tianjin Fengchuan Chemical Co., Ltd. and Tianjin Fuyu Chemical Co., Ltd., respectively. These chemical reagents were used as received without further purification.

2.2 Preparation of PI

TFDB (6.4046 g, 0.02 mol) was dissolved in DMAc (92 mL) under nitrogen flow and added with 6FDA (8.8885 g, 0.02 mol) at room temperature. After reaction for 24 h, acetic anhydride (6 mL) and triethylamine (3 mL) were added to the solution and stirred for 12 h. The solution was then poured into absolute ethyl alcohol for precipitation. The precipitates were separated through filtration and washed three times with ethyl alcohol to completely remove the salts. The products were dried in a vacuum oven overnight at 50 °C. The polymerization route of PI is shown in Scheme 1.

2.3 Preparation of PI nanofoams

PI powder and PEG-600 were added to a flask with DMAc (10 mL), stirred for 4 h, and sonicated for 2 h. PI solutions with different contents of PEG-600 were coated on glass by a doctor blade and heated at 80 °C for 12 h and at 300 °C for 1 h in nitrogen atmosphere. The films were cooled to room temperature and heated again at 260 °C for 20 h and at 300 °C for 2 h in air to fabricate PI nanofoams.

2.4 Characterization

Fourier transform infrared (FTIR) spectra were recorded on a VERTEX 70 spectrometer. Thermogravimetric analysis (TGA) was conducted from room temperature to 800 °C at a heating rate of 10 °C min^{-1} under nitrogen atmosphere or air atmosphere by using Perkin-Elmer Diamond TG/DTA equipment. Scanning electron microscopy (SEM) was performed at an acceleration voltage of 10 kV to visualize the cross-sectional morphology of the films. Dynamic mechanical analysis (DMA) was conducted on a Rheometric scientific DMTA-V at 1 Hz with a heating rate of 10 °C min^{-1} within 50 °C to 450 °C. The density of PI nanofoams was determined by a densitometer (YAK01-OD). The dielectric constants of PI nanofoams were measured by a Concept 80 Broadband Dielectric Spectrometer within −150 °C to 150 °C from 1 Hz to 10^6 Hz. The molecular weights (M_n) and molecular weight distributions (PDI) of the PI/PEG composite and PI nanofoam were determined using gel permeation chromatography (GPC) equipped with a Waters 515 pump, Waters 717 plus autosampler, PL gel MIXED-BLS columns (300 × 7.5 mm, 10 μm) and Waters 2414 differential refractive index detector at 35 °C, with monodispersed polystyrene as the calibration standard. Dimethyl formamide containing 0.1 wt% tetrabutyl-ammonium bromide was used as the eluent at a flow rate of 1.0 mL min^{-1}.

3. Results and discussion

3.1 Preparation of PI nanofoams

Typically, PI solutions were prepared by the reaction of TFDB with 6FDA in DMAc, followed by mixing with PEG-600 to obtain PI/PEG composite films. Finally, the composite films were heated to prepare PI nanofoams. Fig. S1a and b† show the FTIR curves of PEG-600 and pure PI film. Comparing the above two curves, the characteristic absorption peaks of PEG-600 and pure PI film were overlapped except the peaks of PEG-600 at 2920 cm^{-1} and 3400

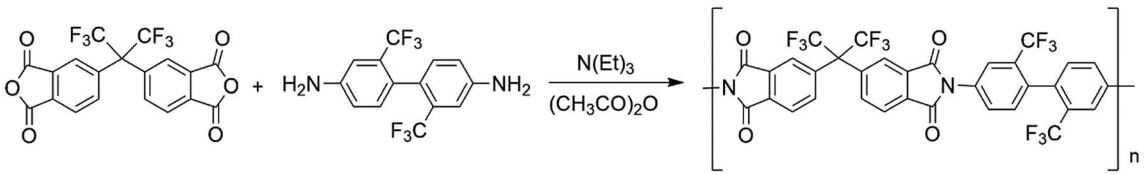

Scheme 1 Polymerization route of the PI.

cm^{-1}, which are attributed to the –CH_2– group and adsorbed water in air, respectively. Fig. S1c† presents the characteristic absorption peaks of imide rings at 1726 cm^{-1} (ν_{sym}C═O), 1786 cm^{-1} (ν_{asym}C═O), and 1363 cm^{-1} (ν_{CN}imide); the peaks of PEG-600 at 2920 cm^{-1} (–CH_2– group) are well defined, indicating that the PI/PEG composite films were successfully prepared. However, strong absorption bands were observed at 2900 to 3200 cm^{-1}, which are assigned to COOH and NH_2 groups (Fig. S1c†); these bands are caused by incomplete imidization of the PI/PEG composite films by the chemical method. Prior to conversion into PI nanofoams, the PI/PEG composite films were heated to be imidized totally in nitrogen atmosphere. Fig. S1d† depicts a peak at 2920 cm^{-1}, which belongs to PEG disappearance. All the characteristic peaks of PI are well defined, indicating successful preparation of PI nanofoams.

It was reported that in order to obtain the PI nanofoams *via* the thermolysis method, the thermal decomposition temperature of labile content should be lower than the T_g of the PI resin matrix to obtain PI nanofoams through thermolysis; the temperature of imidization should be lower than the temperature of labile content thermolysis.[29] PEG-600 started to decompose at 175 °C in air atmosphere while at 335 °C in nitrogen atmosphere (Fig. S2†). And the T_g and temperature of imidization of the PI matrix (6FDA/TFDB) are 324 °C and 300 °C, respectively, indicating that the PI nanofoams could be prepared by thermolysis of the PI/PEG composites. As shown in Fig. 1, TGA curve of pure PI film displayed one stage, and the curve of the PI/PEG composite film showed two stages of weight loss. According to Fig. S2,† PEG started to decompose at 335 °C in nitrogen atmosphere. The results indicated that the first weight loss stage of the TGA curve of the PI/PEG composite film is associated with the decomposition of the PEG chain, and the other stage is related to the decomposition of the PI backbone. The TGA curve of the PI nanofoam shows one stage of weight loss, and the highest decomposition rate was detected at 600 °C. These findings indicate that the nanofoam has the same decomposition temperature as that of the pure PI film. Hence, PI nanofoams were prepared successfully.

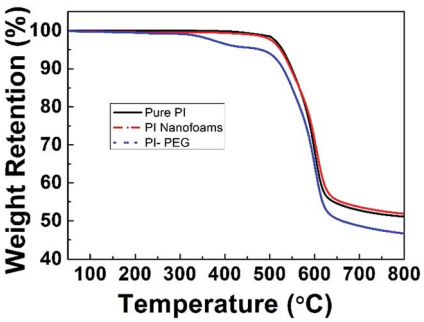

Fig. 1 TGA curves of pure PI film, PI/PEG composite film (10 wt%) and PI nanofoams in nitrogen atmosphere.

Cross-sectional morphologies of pure PI film and PI nanofoams prepared by thermolysis of PI/PEG composite films with different PEG contents were observed by SEM analysis. According to Fig. 2a, pure PI film showed a smooth view and no nanopores were observed; PI nanofoam after 5 wt% PEG removal revealed more nanopores clearly (Fig. 2b). The nanopores are uniform and regular in shape. As seen in Fig. 2, the average diameters of the nanopores are approximately 97 nm, 138 nm and 164 nm respectively, associated to the removed PEG content of 5 wt%, 15 wt% and 20 wt%. Obviously, as the removed PEG content increasing from 5 wt% to 20 wt%, the average diameters of the nanopores increase because of PEG accumulation. Notably, numerous nanopores were not observed in the cross-sectional SEM micrographs because partial nanopores were destroyed when the samples were prepared *via* brittle fracture in liquid nitrogen.

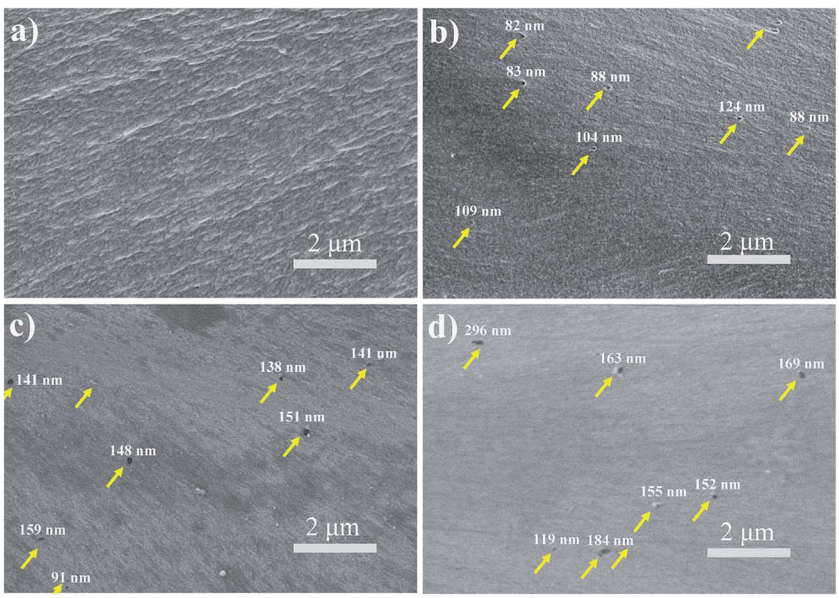

Fig. 2 Cross-sectional SEM micrographs of PI nanofoams after removal of the PEG content of (a) 0 wt%, (b) 5 wt%, (c) 15 wt%, and (d) 20 wt%.

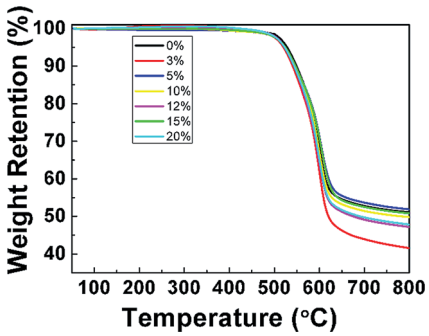

Fig. 3 TGA curves of PI nanofoams after removal of PEG with different content.

3.2 Thermal properties of PI nanofoams

TGA and DMA measurements were performed to investigate the thermal properties of pure PI film and PI nanofoams. According to the TGA results (Fig. 3), PI nanofoams prepared after removal of PEG with different contents, namely, 3, 5, 10, 15, and 20 wt%, showed similar decomposition temperature to that of pure PI. Table S1† shows that the average temperatures at which PI nanofoams exhibited 5% and 10% weight loss are 523 °C and 545 °C, respectively; and the corresponding temperatures of pure PI film are 528 °C and 549 °C, respectively. Hence, the fabricated PI nanofoams maintained excellent thermal stabilities.

The dynamic mechanical properties of pure PI film and PI nanofoams are shown in Fig. 4. With temperature increasing, two peaks were observed on the tan δ curve of the pure PI film, indicating that two transition phases existed. The first transition at the temperature range of 150 °C to 280 °C is related to β relaxation, which is attributed to the movement of the small group of PI chains. The second transition at the temperature range of 280 °C to 450 °C is due to the movement of macromolecular chain segments, which is related to glass transition. The peak temperatures of the two transitions are 243 °C and 338 °C, respectively. The as-prepared PI nanofoams showed a similar transition behavior to that of the pure PI film. The average peak temperatures of β relaxation and T_g for PI nanofoams are 243.5 °C and 344.3 °C, respectively; these PI nanofoams display good thermal properties similar to the pure PI film (Table 1).

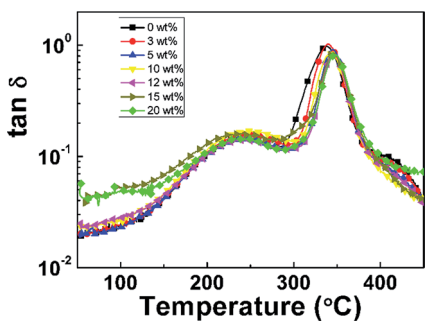

Fig. 4 DMA curves of PI nanofoams after removal of PEG with different content.

Table 1 Thermal properties of PI nanofoams prepared by the thermolysis of PI/PEG composite films with different PEG content *via* DMA measurements

PEG content (wt%)	T_β (°C)	T_g (°C)
0	243	338
3	245	339
5	245	345
10	248	341
12	241	346
15	241	346
20	241	349

3.3 Dielectric properties of PI nanofoams

3.3.1 Effect of porosity on the dielectric properties. The porosity of PI nanofoams was calculated by density methods[10] to investigate the effect of porosity on the dielectric constant (Table 2 and Fig. S3†). With increasing PEG content from 0 wt% to 20 wt% in the PI matrix, the porosity of PI nanofoams prepared by thermolysis of PI/PEG composite films increased from 0% to 7.6%. The dielectric constants of the PI nanofoams with different porosity levels were calculated according to Maxwell-Garnett theory[30] in the following equation:

$$\varepsilon = \varepsilon_2 = \left(\frac{\varepsilon_1 + 2\varepsilon_2 + 2P(\varepsilon_1 - \varepsilon_2)}{\varepsilon_1 + 2\varepsilon_2 - P(\varepsilon_1 - \varepsilon_2)}\right) \quad (1)$$

where P is porosity; and ε, ε_1, and ε_2 are the dielectric constants of PI nanofoams, PI matrix, and air, respectively. As shown in Table 2, the dielectric constant of the PI nanofoams calculated by density method decreased from 2.89 to 2.71 as the porosity level increased from 0% to 7.6%. Furthermore, the dielectric constants of the PI nanofoams were measured directly by dielectric spectrometer. As shown in Fig. 5, the dielectric constant of the PI nanofoams significantly decreased from 2.8 to 2.4 at 1 MHz as the porosity increased from 0% to 7.6%. The calculated values of the dielectric constant of PI nanofoams are consistent with the measured values at low porosity levels. However, with the porosity increasing from 6.59% to 7.6%, the calculated values are higher than the measured results. With increasing PEG content, the pores of the PI nanofoams were connected partially to form through holes, leading to the permeation of the large amount of water to the PI nanofoams. As a result, the measured density of the PI nanofoams increased

Table 2 Density, porosity and dielectric constant of PI nanofoams

PEG content (wt%)	Density (g cm^{-3})	Porosity[a] (%)	ε^a	ε^b
0	1.533	0	2.89	2.91
3	1.496	2.40	2.83	2.89
5	1.475	3.80	2.79	2.85
10	1.465	4.46	2.78	2.78
12	1.450	4.86	2.76	2.73
15	1.432	6.59	2.73	2.53
20	1.417	7.60	2.71	2.49

[a] Calculated by density method. [b] Measured by dielectric spectrometer at 1 Hz.

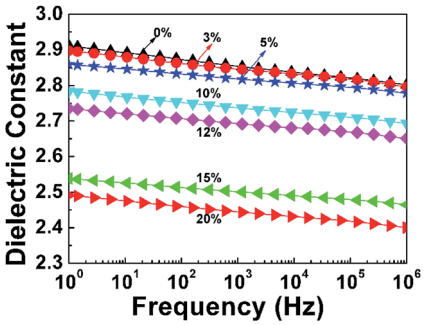

Fig. 5 Dielectric constant of pure PI film and PI nanofoams after removal of PEG with different content in the frequency range of 1 Hz to 1 MHz.

and the calculated porosity decreased, leading to increased dielectric constant values. Additionally, only a slight decrease of dielectric constants of the PI nanofoams with the increase of frequency was observed, which demonstrated the dielectric constant of the as-prepared PI nanofoams with different porosities was stable in the wide frequency range.

3.3.2 Thermal stability of the dielectric properties. Generally, microelectronics devices undergo high and ultra-low temperatures during manufacturing operations, such as soldering and quenching, which require dielectric properties of interlevel dielectrics between the layers of wire to show excellent thermal stability. Thus, the dielectric constant of PI nanofoams was determined within −150 °C to 150 °C at 1 MHz to investigate the thermal stability of dielectric properties of the nanofoams in present work. Before measuring the dielectric constant, the samples were heated at 120 °C for 30 min to remove water. As shown in Fig. 6, the dielectric constants of both pure PI film and PI nanofoams after removal of 15 wt% PEG exhibited stable values at 2.81 and 2.46, respectively, in the entire temperature range. However, at 0 °C, the dielectric constant for both pure PI and PI nanofoams slightly fluctuated because of little water adsorption. In general, the results demonstrate that the as-prepared nanofoams could be applied in integrated circuit fields in the temperature range of −150 °C to 150 °C.

3.3.3 Effect of thermal treatment process on the dielectric properties. According to literature,[14,16] the PI matrix would be plastified by products of thermal decomposition in the process of preparation for the PI nanofoams, which could cause a negative impact on the dielectric properties. If the escape rate of the products of PEG decomposition was slower than its decomposition rate, the time for the decomposition products to escape would be insufficient. Consequently, the PI matrix could be plastified by gas produced by PEG decomposition, which caused the T_g of the PI matrix to decrease and nanopores to collapse. To eliminate the negative effects, four procedures for thermal treatment of PI/PEG composite films were designed and conducted, which were designated as procedure 1, 2, 3, and 4 respectively. Specifically, in procedure 1, the PI/PEG composite films were heated directly at 260 °C for 20 h and 300 °C for 2 h. In procedure 2, the composite films were heated with the temperature increasing from 25 °C to 300 °C at a heating rate of 5 °C min^{-1}, followed by heating at 300 °C for 1 h. In procedure 3, the composite films were heated at 175 °C, 225 °C, 250 °C, and 300 °C for 1 h at a heating rate of 5 °C min^{-1}. In procedure 4, the composite films were heated at 175 °C, 225 °C, 250 °C, and 300 °C for 1 h at a heating rate of 1 °C min^{-1}. According to the isothermal TGA analysis of PI/PEG composite film shown in Fig. S4,† the mass of the PI/PEG composite film decreased sharply when heated from 0 to 400 min at 260 °C, and the highest mass loss rate occurred at 100 min. Then, a slow decline of the mass loss was observed with the increase of heating time. When the heating time was raised to 1200 min, the mass loss of PI/PEG composite film remained constant. The results of the isothermal TGA analysis of PEG-600 further demonstrated that PEG-600 could be decomposed completely in the PI matrix in the present work. As shown in Fig. 7, the dielectric constants of PI nanofoams after removal of 15 wt% PEG obtained by four procedures in the sequence are 2.46, 2.25, 2.14, and 2.12 at 1 MHz. It is clear that PI nanofoams prepared by procedure 1 showed the largest dielectric constant value. This was because the escape rate of decomposition products was too fast, and there was insufficient time to generate more pores. Compared with procedure 1, procedure 2 had a relatively lower thermal decomposition rate, and the dielectric constant value was lower than the value of procedure 1. Compared with procedure 2, raising the temperature in stages was adopted in

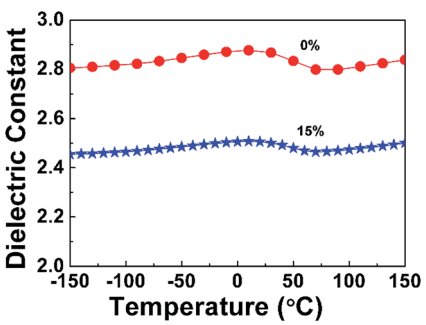

Fig. 6 Effect of temperature on the dielectric constant of pure PI film and PI nanofoams after removal of 15 wt% PEG at the frequency of 1 MHz.

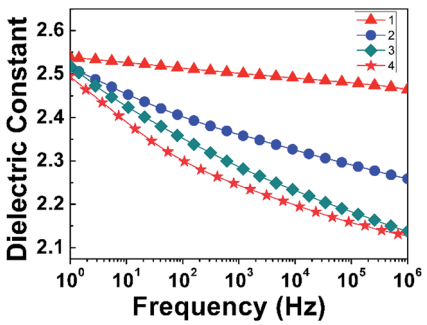

Fig. 7 Effect of thermal treatment conditions on dielectric constant of PI nanofoams after removal of 15 wt% PEG in the frequency range of 1 Hz to 1 MHz.

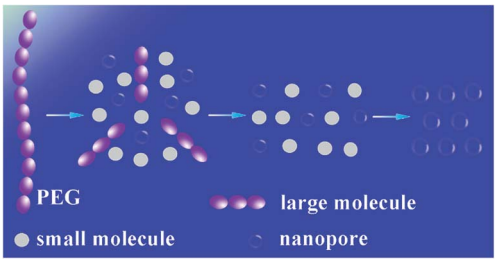

Scheme 2 The schematic of the process of PEG thermal decomposition.

procedure 3 to obtain improved dielectric properties. On the basis of procedure 3, we further reduced the heating rate of the composite films to slow the decomposition rate of PEG, thereby successfully obtaining PI nanofoams with the lowest dielectric constant.

In order to investigate the thermal process, the PI/PEG composite film and PI nanofoam with PEG decomposed partly were measured in GPC. According to Fig. S5,† the M_n and PDI of PI showed no changes before and after thermal decomposition process. For the PI/PEG composite film, there was a single peak belonged to PEG in the GPC curve. However, two peaks of PEG appeared in the GPC curve of PI nanofoam with PEG decomposed partly. The corresponding PDI of PEG before and after thermal decomposition process showed an obvious increase from 1.03 to 1.06. The above process of PEG thermal decomposition was illustrated in Scheme 2. The PEG macromolecular chain first decomposed to large-molecule chains and small molecules which were easily volatilized without shell or other precipitates in the heated condition. Second, the macromolecular chains gradually decomposed to volatile small molecules. In this process, the small molecules accumulated to escape from the matrix resulting in the formation of the nanopores. Thus, the volatile molecules need sufficient time to escape. Otherwise, the PI matrix would be plastified by the products, which caused the collapse of partial holes. When the decomposition rate of thermal labile content is balanced to the escape rate of its decomposition products, PI nanofoams show better dielectric properties.[31]

4. Conclusions

PI nanofoams with low dielectric constant were prepared successfully by introducing pores into the PI matrix containing fluorine groups *via* thermolysis of PEG. The as-prepared PI nanofoams showed nanosized closed pores and retained their excellent thermal stability in excess of 550 °C. With the increase of PEG content, the porosity of PI nanofoams increased, and a significant decrease for the dielectric constant, from 2.80 to 2.12, was observed. We also found that the dielectric constant of the nanofoams was stable at 2.46 in the temperature range of −150 °C to 150 °C. Controlling the thermal decomposition procedure to improve the dielectric properties is effective. The dielectric constant of the PI nanofoams was clearly reduced from 2.4 to 2.12 with decreasing heating rate. PI nanofoams exhibited improved dielectric properties when the decomposition rate of PEG was balanced to the diffusion rate of the decomposition products of PEG. Excellent thermal properties and dielectric properties of PI nanofoams could improve performances on electronic circuitry transmission and display limitless applications in the field of microelectronics.

Acknowledgements

The authors thank the National Basic Research Program of China (973 program, Key Project: 2014CB643604).

References

1 H. Treichel, G. Ruhl, P. Ansmann, R. Würl, C. Müller and M. Dietlmeier, *Microelectron. Eng.*, 1998, **40**, 1–19.
2 J. Hedrick, K. Carter, J. Labadie, R. Miller, W. Volksen, C. Hawker, D. Yoon, T. Russell, J. McGrath and R. Briber, in *Progress in Polyimide Chemistry II*, Springer, 1999, pp. 1–43.
3 K. Maex, M. Baklanov, D. Shamiryan, S. Brongersma and Z. Yanovitskaya, *J. Appl. Phys.*, 2003, **93**, 8793–8841.
4 International Technology Roadmap for Semiconductors Reports, The international technology roadmap for semiconductors, http://www.itrs2.net/itrs-reports.html, 2009.
5 G. Maier, *Polym. Sci.*, 2001, **26**, 3–65.
6 B. Sillion, R. Mercier and D. Picq, *Synthetic methods in step-growth polymerisation*, John Wiley & Sons, New York, 2003, pp. 265–319.
7 H. Deligöz, T. Yalcinyuva, S. Özgümüs and S. Yildirim, *Eur. Polym. J.*, 2006, **42**, 1370–1377.
8 A. Stich, Z. Gabric and W. Pamler, *Microelectron. Eng.*, 2005, **82**, 362–367.
9 B. D. Hatton, K. Landskron, W. J. Hunks, M. R. Bennett, D. Shukaris, D. D. Perovic and G. A. Ozin, *Mater. Today*, 2006, **9**, 22–31.
10 K. R. Carter, H. J. Cha, R. A. Dipietro, C. J. Hawker, J. L. Hedrick, J. W. Labadie, J. E. Mcgrath, T. P. Russell, M. I. Sanchez, S. A. Swanson, W. Volksen, D. Y. Yoon, *MRS Proceedings*, Cambridge University Press, 1995, vol. 381, p. 79.
11 Y. Charlier, J. L. Hedrick, T. Russell, S. Swanson, M. Sanchez and R. Jérôme, *Polymer*, 1995, **36**, 1315–1320.
12 J. Hedrick, R. DiPietro, Y. Charlier and R. Jerome, *High Perform. Polym.*, 1995, **7**, 133–147.
13 C. Plummer, J. L. Hedrick, H. H. Kausch and J. Hilborn, *J. Polym. Sci., Part B: Polym. Phys.*, 1995, **33**, 1813–1820.
14 J. L. Hedrick, T. Russell, M. Sanchez, R. DiPietro, S. Swanson, D. Mecerreyes and R. Jérôme, *Macromolecules*, 1996, **29**, 3642–3646.
15 J. Fodor, R. Briber, T. Russell, K. Carter, J. Hedrick, R. Miller and A. Wong, *Polymer*, 1999, **40**, 2547–2553.
16 J. L. Hedrick, C. J. Hawker, R. DiPietro, R. Jérôme and Y. Charlier, *Polymer*, 1995, **36**, 4855–4866.
17 S. Y. Cho, C. H. Lee, S. Y. Oh and C. M. Chung, *Ultramicroscopy*, 2008, **108**, 1220–1223.

18 J. L. Hedrick, K. Carter, H. Cha, C. Hawker, R. DiPietro, J. Labadie, R. Miller, T. Russell, M. Sanchez and W. Volksen, *React. Funct. Polym.*, 1996, **30**, 43–53.
19 J. L. Hedrick, T. Russell, J. Labadie, M. Lucas and S. Swanson, *Polymer*, 1995, **36**, 2685–2697.
20 J. L. Hedrick, J. Labadie, T. Russell, D. Hofer and V. Wakharker, *Polymer*, 1993, **34**, 4717–4726.
21 J. L. Hedrick, K. Carter, R. Richter, R. Miller, T. Russell, V. Flores, D. Meccereyes, P. Dubois and R. Jerome, *Chem. Mater.*, 1998, **10**, 39–49.
22 J. L. Hedrick, R. Dipietro, C. Plummer, J. Hilborn and R. Jérôme, *Polymer*, 1996, **37**, 5229–5236.
23 S. H. Han, J. S. Do, M. A. Kader, J. H. Lee, M. H. Lee and C. Nah, *Polym. Adv. Technol.*, 2004, **15**, 370–376.
24 S. Mehdipour-Ataei and S. Saidi, *e-Polym.*, 2007, **7**, 1291–1301.
25 Y. Chen, W. Wang, W. Yu, Z. Yuan, E. T. Kang, K. G. Neoh, B. Krauter and A. Greiner, *Adv. Funct. Mater.*, 2004, **14**, 471–478.
26 G. Fu, W. Wang, S. Li, E. Kang, K. Neoh, W. Tseng and D. Liaw, *J. Mater. Chem.*, 2003, **13**, 2150–2156.
27 Y. H. Zhang, L. Yu, L. H. Zhao, W. S. Tong, H. T. Huang, S. M. Ke and H. Chan, *J. Electron. Mater.*, 2012, **41**, 2281–2285.
28 Y. Zhang, S. Ke, H. Huang, L. Zhao, L. Yu and H. L. Chan, *Appl. Phys. Lett.*, 2008, **92**, 1–3.
29 K. R. Carter, R. A. DiPietro, M. I. Sanchez and S. A. Swanson, *Chem. Mater.*, 2001, **13**, 213–221.
30 H. J. Chu, B. K. Zhu and Y. Y. Xu, *J. Appl. Polym. Sci.*, 2006, **102**, 1734–1740.
31 Y. Charlier, J. Hedrick, T. Russell, A. Jonas and W. Volksen, *Polymer*, 1995, **36**, 987–1002.